Cyclic test data of two mixed RC-URM wall structures

Alessandro Paparo and Katrin Beyer

Earthquake Engineering and Structural Dynamics Laboratory (EESD), School of Architecture, Civil and Environmental Engineering (ENAC), École Polytechnique Fédérale de Lausanne (EPFL)

1 Introduction

This document provides additional information on the two quasi-static cyclic tests carried out at EPFL on two mixed reinforced concrete-unreinforced masonry (RC-URM) wall structures. The first part of the document outlines the test objectives and the organisation of the data, which are available to the public. In the second part, additional photos of the two specimens, showing the evolution of the crack patterns, are provided.

2 Test objectives

The test campaign focuses on the seismic behaviour of mixed RC-URM wall structures representative of residential buildings in Switzerland (their detailed description is presented in the introduction of the thesis). Although such mixed systems are rather common in countries of low to moderate seismicity, current seismic design codes do not address such mixed structures. It is believed that the development of guidelines has been hindered by the lack of experimental evidence, against which numerical and mechanical models could be validated.

To improve the understanding of such mixed systems, a research programme was started at EPFL. Within this programme, two quasi-static cyclic tests on two-third scale models (TU1 and TU2) representing a prototype structure have been carried out. The two storey specimens are composed of one RC wall coupled to a one URM wall by two RC beams (Figures 1 and 2). For a detailed

description of the specimens and the test set-up, the reader is referred to Paper I. The objectives of this test campaign were *(i)* to measure the distribution of the reaction forces between the walls, *(ii)* to understand the influence of the interaction between RC and URM walls on the global behaviour of mixed systems, *(iii)* to identify typical features related to such structures and *(iv)* to collect data that can be used for the validation of numerical models.

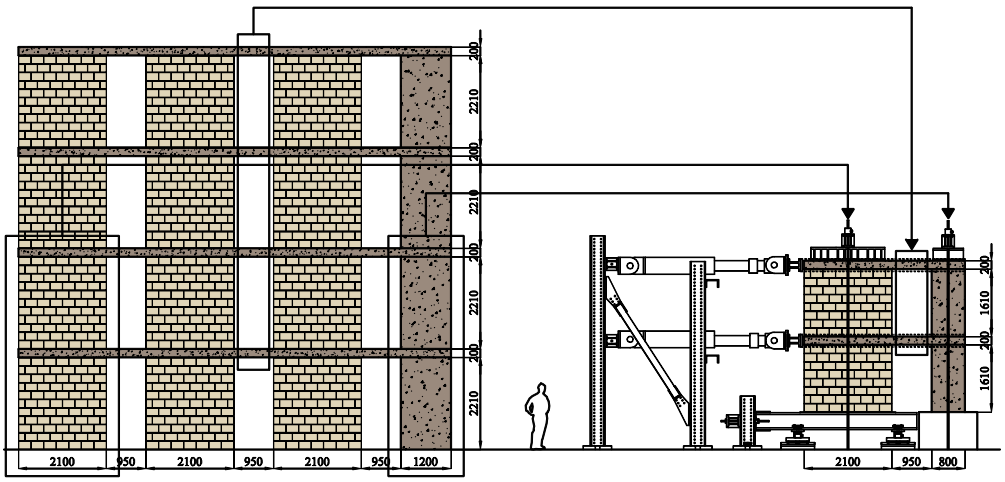

Figure 1: Reference structure and test unit. The elements of the reference structure represented in the test unit are encircled (all dimensions in mm).

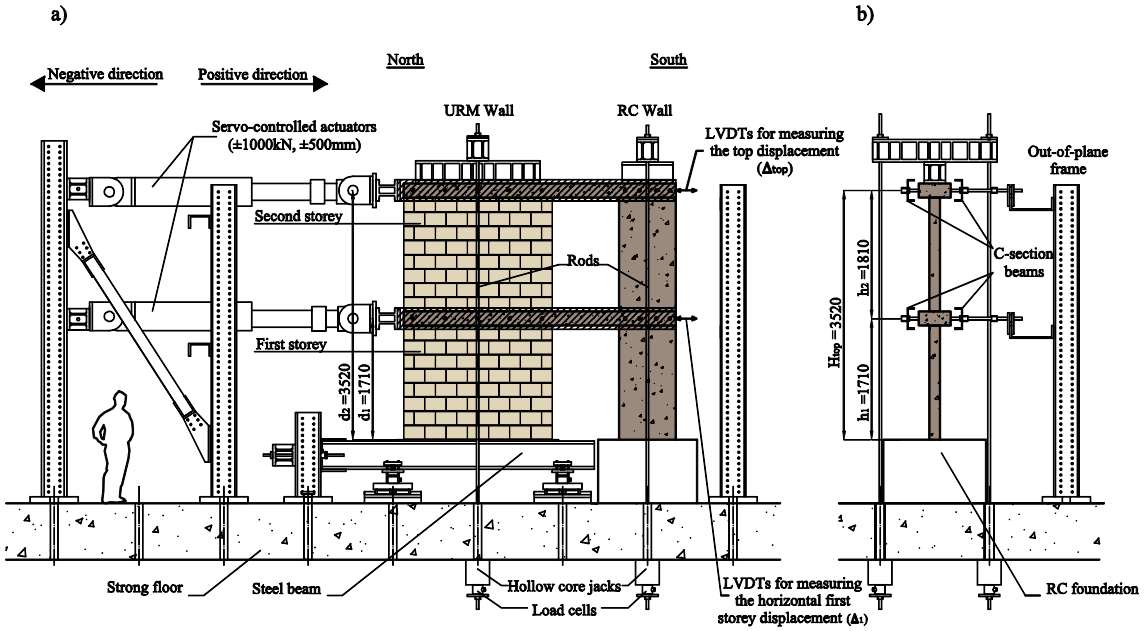

Figure 2: Test set-up. (a) front view; (b) side view. All dimensions in mm.

3 Organisation of the test data

This part of the document presents the experimental data gathered from the two tests. Section 3.1 specifies the instruments used during the tests to monitor global and local quantities. Section 3.2 follows with a description of the organisation of the folders containing photos and data.

3.1 Instrumentation

The two specimens (TU1 and TU2) were instrumented with a series of conventional measurement devices (i.e., load cells, LVDTs, strain gauges and omega gauges). Figure 3 shows the instrumentation used for calculating the global quantities (i.e., the reaction forces at the base of the walls, the storey displacements and the foundation displacements). Next to global quantities, elongations and shear deformations of the RC walls were measured with LVDTs (Figures 4a and 4b). Positive values from the LVDTs correspond to a shortening of the base length of the measurement. Concerning the measurement of the shear deformations of the RC walls, the positions of Diag3, Diag4, Diag7 and Diag8 were slightly changed from TU1 to TU2. Figure 4b represents the instrumentation layout of TU1 with solid lines and the instrumentation layout modified for TU2 with dashed lines. In TU2, the sliding of the RC wall base with respect to the RC foundation was also measured (Figure 4a). A series of strain gauges measured the strain in the central longitudinal reinforcing bars of the RC beams (Figure 5). Positive values from the gauges correspond to tensile strains. Before testing, the strain gauges were checked and, in the positions where the strain gauges were not working, additional omega gauges were installed as presented in Figure 5 (two omega gauges were installed in TU1 and one in TU2). Positive values from the gauges correspond to a shortening of the base length of the measurement.

The deformation pattern of the URM walls was recorded by using the LED-based optical measurement device “Optotrack” from NDI [NDI, 2009]. The system worked with two position sensors. Each of them consists of three digital cameras that record the 3D-coordinates of the LEDs. The LEDs were glued onto the URM wall following a regular 150 mm x 100 mm grid (Figure 6a), except for the LEDs close to the rod and the C-section beams, for which the grid was slightly altered. In Figure 6a, the standard dimensions of the grid are represented only in the bottom-north corner of the URM wall. The figure also shows the dimensions of the altered part of the grid. Additional LEDs were glued onto the steel foundation under the URM wall, the C-section beams and the RC beams (Figures 6a and 6b).

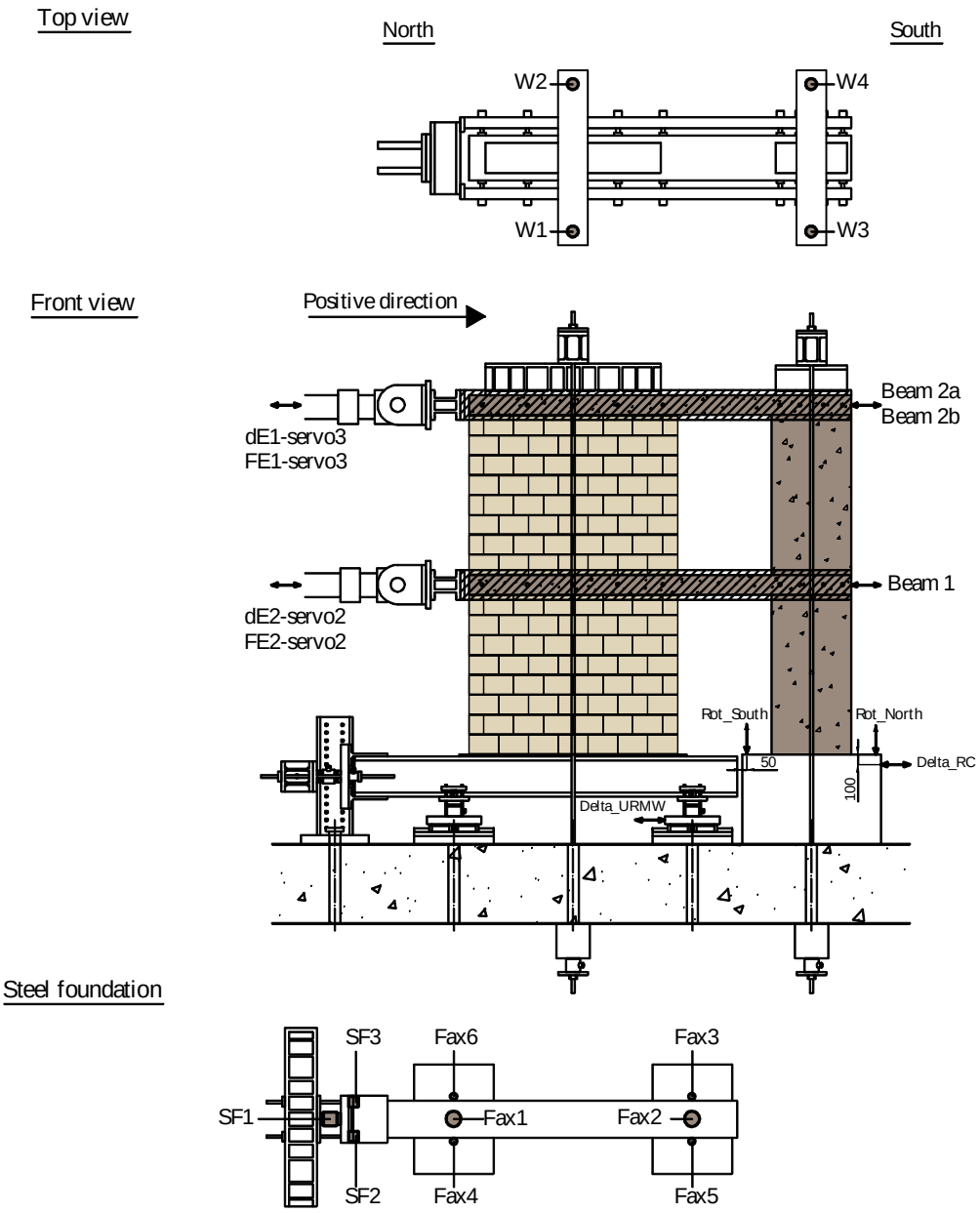

Figure 3: Test set-up with the devices to measure the global response of the specimens and the displacements of the foundations.

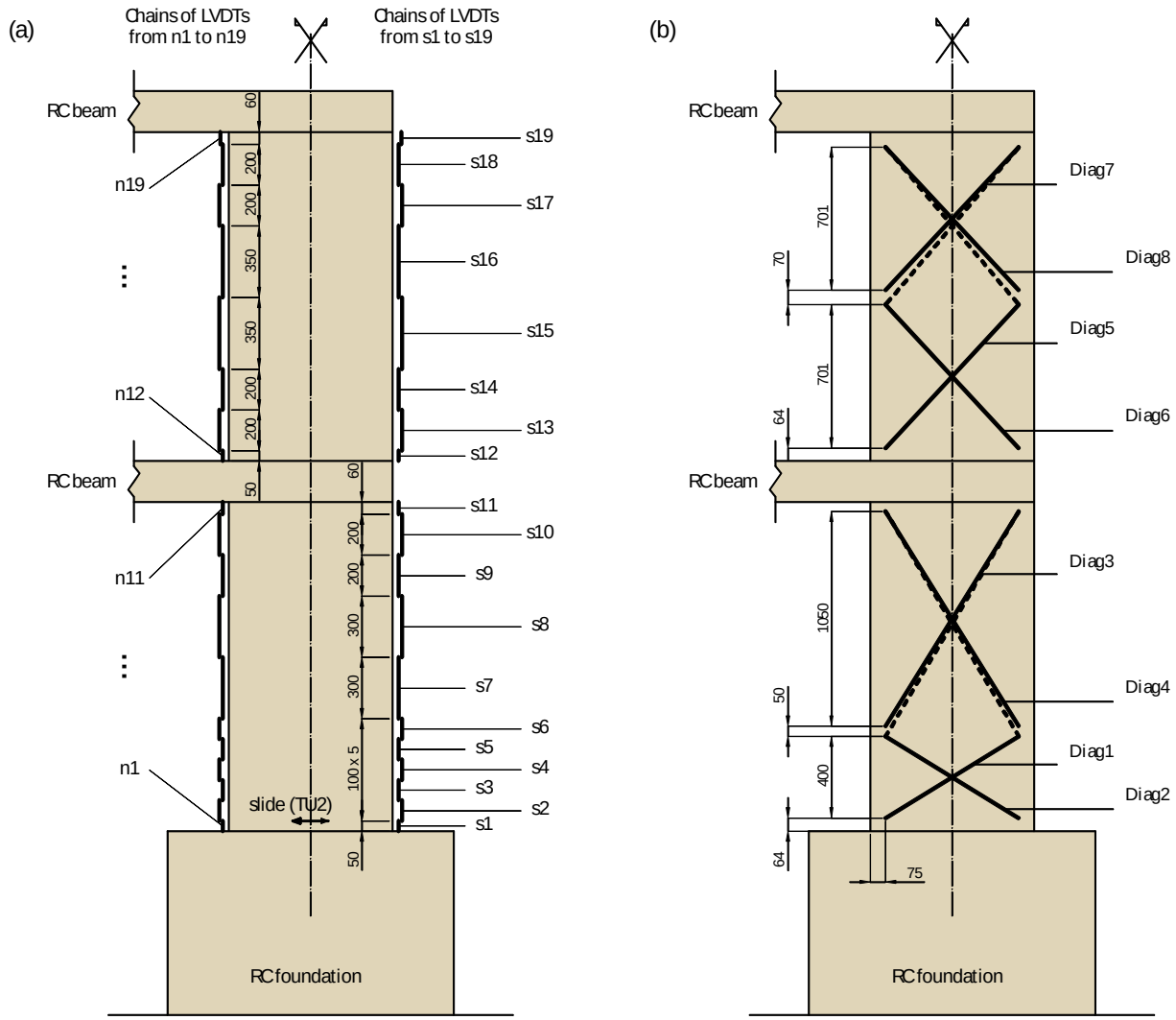

Figure 4: (a) location of the LVDTs to measure the elongation of the edges of the RC wall and the sliding displacement at the RC wall base (TU2 only); (b) LVDTs to measure the shear displacement of the RC wall.

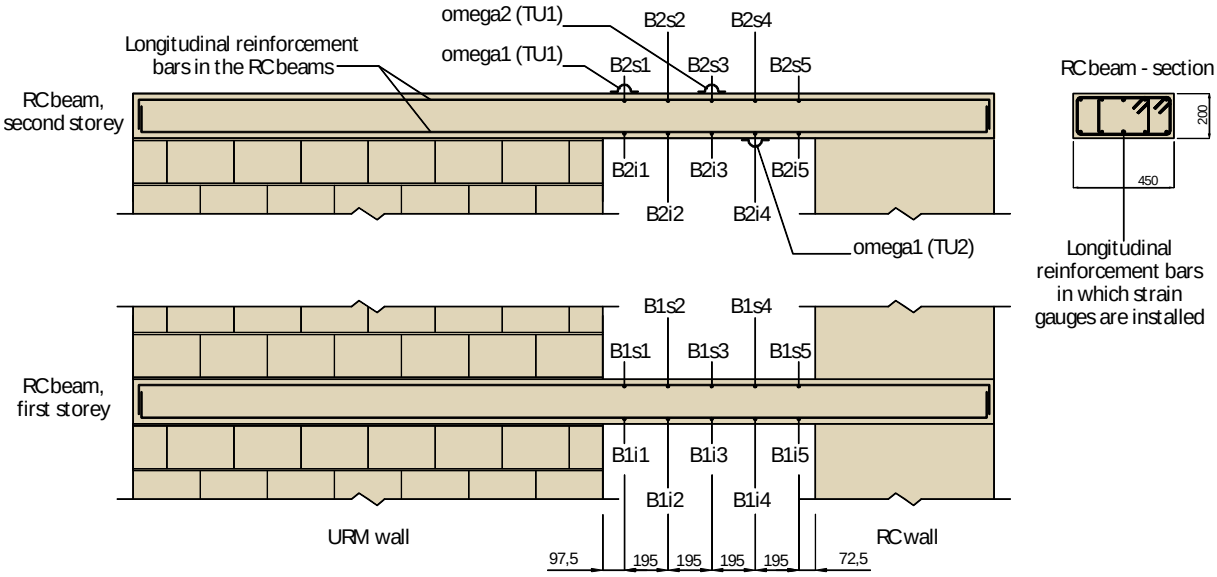

Figure 5: Strain gauges on the reinforcing bars of the RC beams. Omega gauges replacing the strain gauges that were not working in TU1 and TU2.

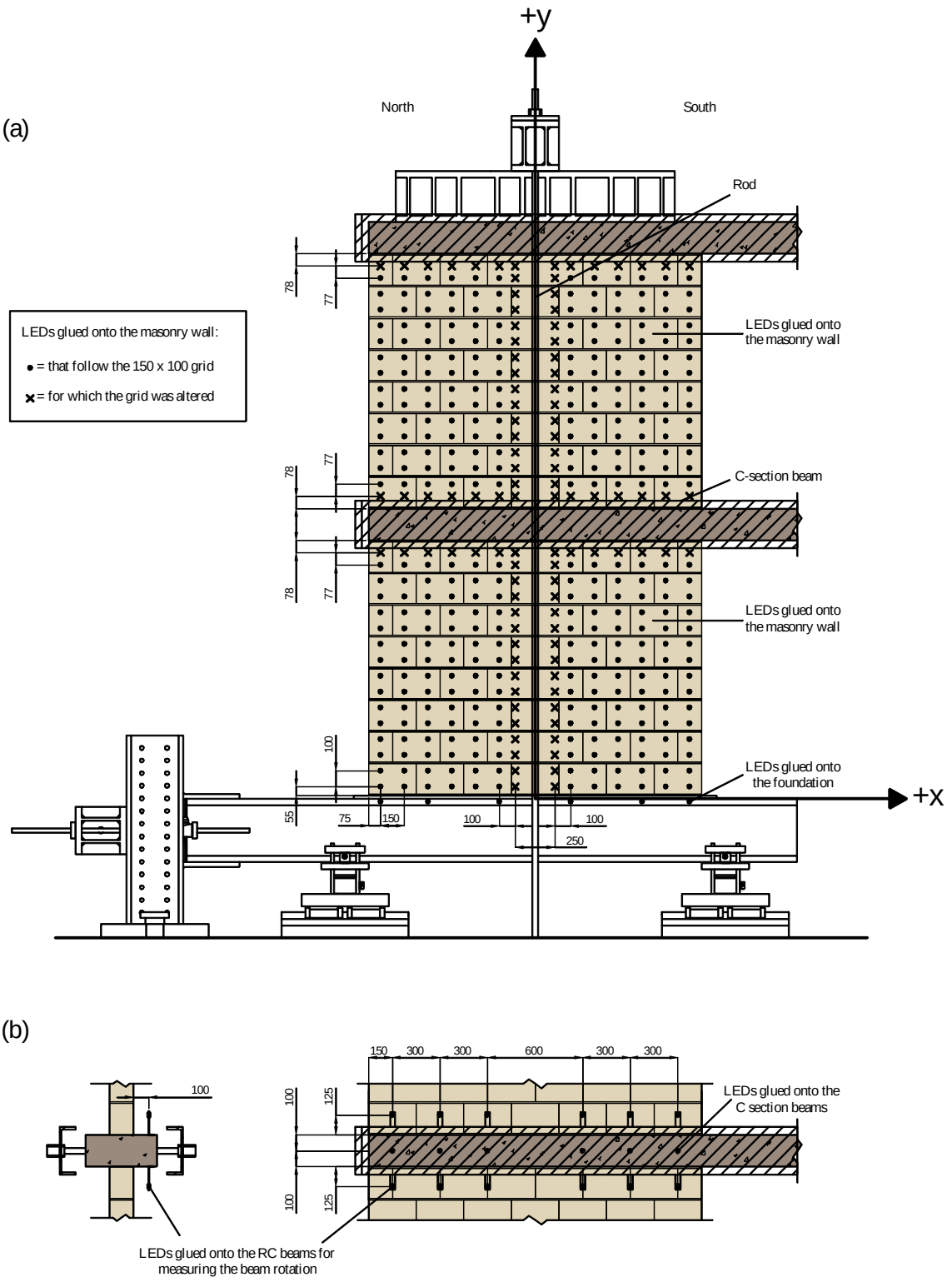

Figure 6: Optical measurement system. (a) LEDs glued onto the URM walls and the steel foundation and sign convention; (b) LEDs glued onto the C-section beams and the RC beams.

3.2 Test data

3.2.1 Data organisation

The data can be downloaded as one zip file from http://eesd.epfl.ch/data_sets. Upon unzipping, the folder structure unfolds as follows (Figure 7). Firstly, the data are organised by specimen (TU1, TU2). For each test unit, there are three folders containing "photos", "unprocessed_data" and "processed_data". In addition, each specimen folder contains one file "metadata_conventional_channels" that contains information on the instruments used.

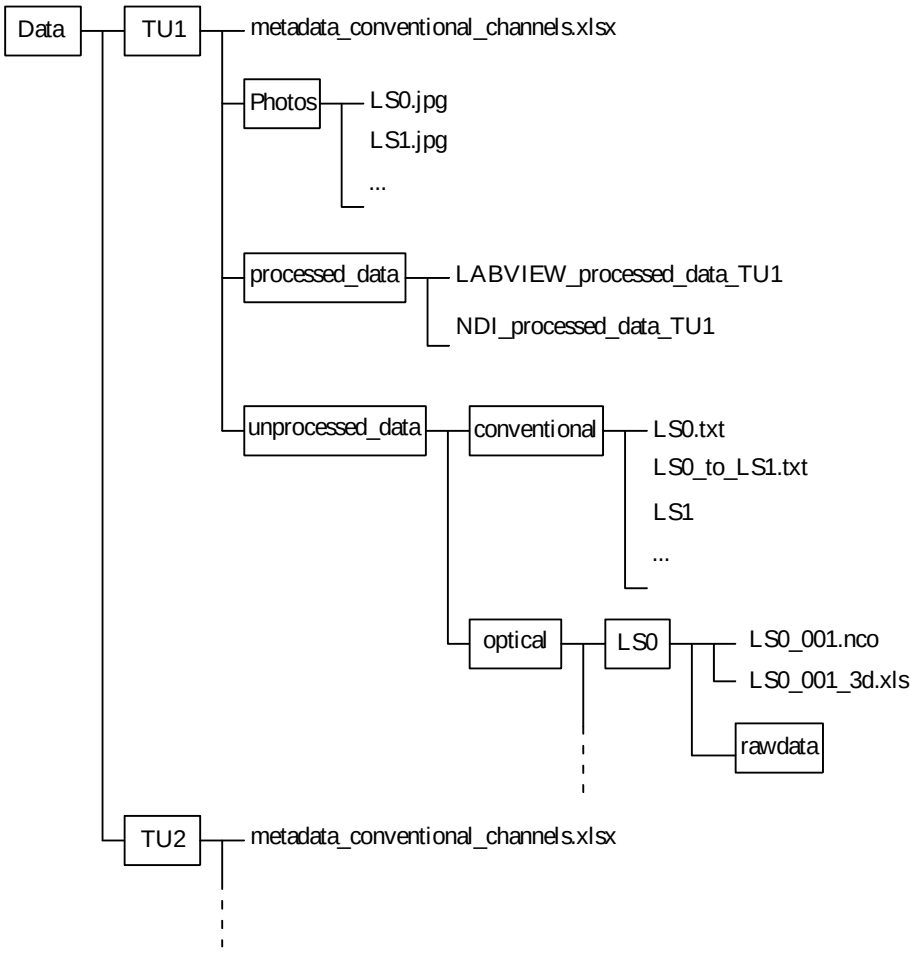

Figure 7: Organisation of the data for TU1 and TU2.

3.2.2 Photos

In addition to the conventional and optical measurements, photos were taken during the test to document the crack pattern of the specimens. Photos are taken at each load step, that is at peak horizontal displacement, and are labelled as "LSxx.JPG", where xx stands for the load step. At each

load step, the cracks were marked with blue and red pens to make them visible in the photos. Cracks that were noticed for the first time at load steps in the positive direction of loading (LS2, LS4, etc.) were marked with blue pens, whereas cracks noticed for the first time at load steps in the negative direction of loading (LS3, LS5, etc.) were marked with red pens. Before the application of the vertical load for TU1, the crane of the laboratory was accidentally hooked up to one C-section beams and uplifted the specimen. This resulted in a horizontal crack running though the top mortar layer of the first storey of the URM wall. This crack was marked in black. However, with the application of the vertical load, this horizontal crack closed and had no influence on the global behaviour of the specimen.

3.2.3 Unprocessed conventional measurement data

The conventional measurements were recorded by using the software LabVIEW (http://www.ni.com/labview/). The files, containing the unmodified outputs of the system, are comprised of the following:

- The measurements of forces and displacements of the two horizontal actuators (FE1-servo3, FE2-servo2, dE1-servo3, dE2-servo2);
- The measurements of axial loads applied at the top of the walls (W1, W2, W3, W4);
- The measurements of the load cells at the base of the URM walls (SF1, SF2, SF3, Fax1, Fax2, Fax3, Fax4, Fax5, Fax6);
- The measurements of the LVDSs (Beam1, Beam2a, Beam2b, n1 to n19, s1 to s19, Diag1 to Diag8, Slide, Rot_North, Rot_South, Delta_RC, Delta_URM);
- The measurements of the strain gauges (B1i1 to B2s5) and of the omega gauges (omega1, omega2);
- The voltage channel "NDI", which was exported from the NDI system to indicate when the optical measurement system was recording. The conventional measurement system was always started before and stopped after the NDI system.

Before the first horizontal load failure (LS27 for TU1 and LS33 for TU2), the measurements are labelled as follows: "LSxx_to_LSxx+1" to indicate the measurement during loading and "LSxx" to indicate the measurement while holding the position at one load step. When the loading is interrupted during the night, the files are labelled as "LSxx_to_0" and "0_to_LSxx+1" and contain the corresponding half load steps with the unloading and the re-loading part.

After the first horizontal failure, the applied horizontal force was held at the maximum value for around one minute and then reduced to zero to avoid the vertical load failure of the specimen during the visual inspection of the unit. As a consequence, the measurements were carried out from zero horizontal force to zero horizontal force (i.e., zero horizontal force → nominal drift → zero horizontal

force). Different labelling for TU1 and TU2 was used, and Figure 8 resumes the names of each measurement with respect to the nominal drift.

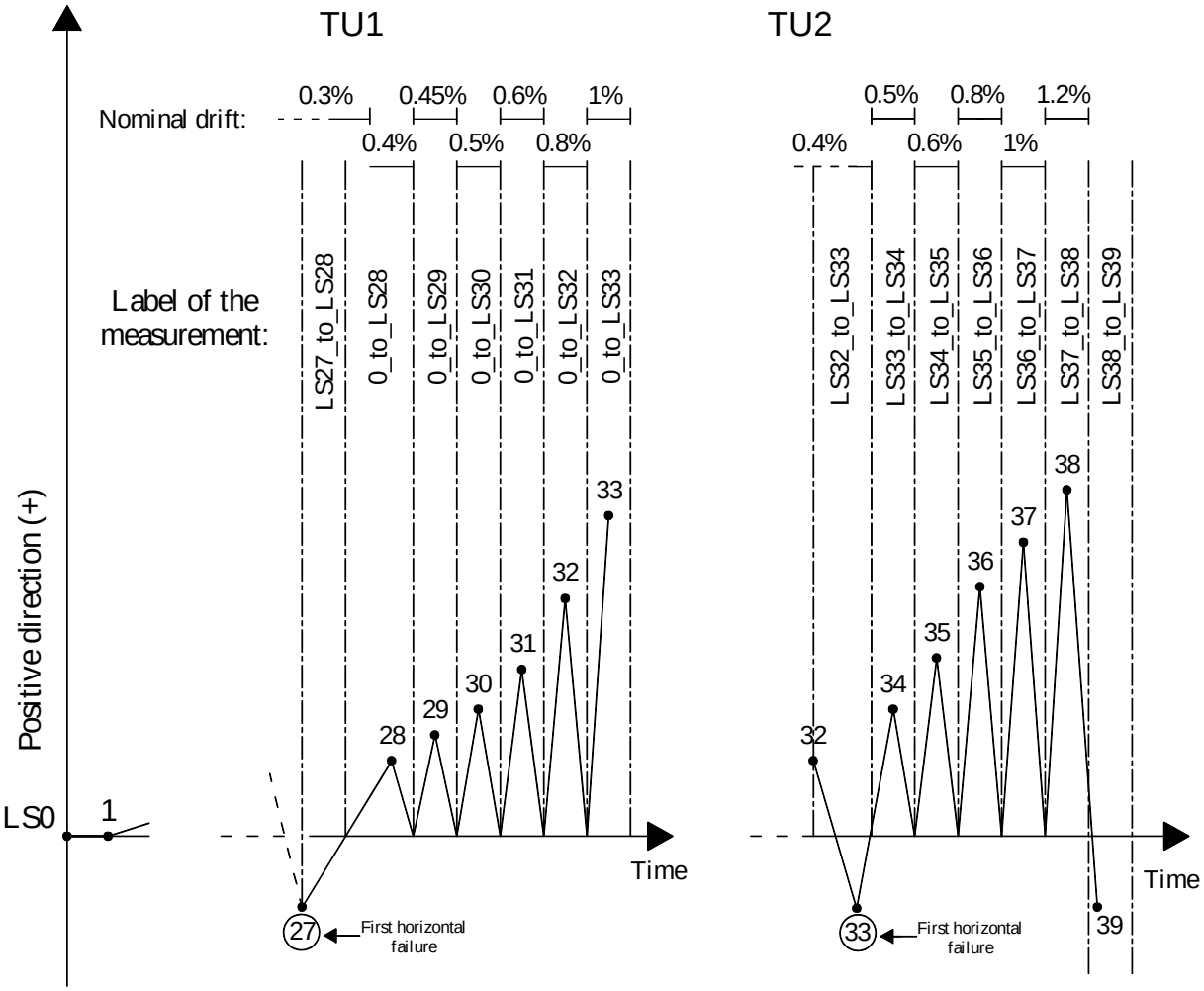

Figure 8: Labels of the measurements for TU1 and TU2 after the first horizontal failure (LS27 and LS33).

3.2.4 Unprocessed optical measurement data

The folder "optical" contains the data measurements from the NDI system. For each recording sequence, the system created a separate folder that contains the data in the specific NDI-format and the measurement data exported to Excel. The folder names are organised as the conventional measurements (e.g., LSxx_to_LSxx+1).

In each Excel-file, the first three lines indicate the included number of frames, the recorder frequency in Hz and the units for the coordinate measurements. After one blank line, the data are organised into columns. The first one contains an index starting from 1. The second and following columns store the x-, y- and z- coordinate for each marker. The labels of these columns are for LED number_1 (Marker_1x, Marker_1y and Marker_1z). At this stage the LED numbers are random. When

the LED coordinates of one marker were not visible to the position sensors, the corresponding columns are blank.

3.2.5 Processed conventional measurement data

The channels measuring the local deformations (n1 to n19, s1 to s19, Diag1 to Diag8, B1s1 to B2i5) were shifted to zero in such a way that the displacement at LS0 corresponds to zero. Furthermore, the conventional data were processed to remove any bias or data that are not linked to the actual behaviour of the test data (e.g., offsets because conventional instruments were moved during testing).

In addition to the recorded channels, a set of computed channels was added to the processed data. The objective of these channels is to allow the user to quickly plot fundamental graphs, such as the base shear-average drift. Table 1 defines the computed channels.

Table 1: Computed channels

Channel number	Channel name	Unit	Formulae / Explanation	Sign convention
114	*index*	-	*Counter of the row*	-
115	*Beam2*	mm	$\frac{Beam2a + Beam2b}{2}$	+ = towards south
116	SF_{urm}	kN	$SF1 + SF2 + SF3$	+ = for positive loading direction (Figure 12)
117	F_e	kN	$FE1 + FE2$	
118	SF_{rc}	kN	$F_e - SF_{urm}$	
119	*N1*	kN	$Fax1 - Fax4 - Fax6$	+ = pushing to bottom
120	*N2*	kN	$Fax2 - Fax3 - Fax5$	
121	*W*	kN	$W1 + W2 + W3 + W4$	
122	*M3*	kNm	$\frac{0.05 \cdot d_m}{2} SF1$	+ = for positive loading direction
123	*N3*	kN	$\frac{2 \cdot N3}{l_h}$	- = pushing to top
124	*ΔN*	kN	$N1 + N2 - N3$	+ = pushing to bottom
125	N_{urm}	kN	$W1 + W2 + \Delta N + 60kN$	
126	N_{rc}	kN	$W3 + W4 - \Delta N + 25kN$	
127	M_{urm}	kNm	$(-N1 + N2) \cdot a + N3 \cdot b + SF_{rc} \cdot c$	+ = for positive loading direction
128	*OTM*	kNm	$FE1 \cdot d_2 + FE2 \cdot d_1$	
129	*Tl*	kNm	$\Delta N \cdot l_{aw}$	
130	M_{rc}	kNm	$Tl - OTM - M_{urm}$	
131	*Drift*	%	$\frac{Beam2}{H_{top}} \cdot 100$	+ = towards south

Beam2 is the average horizontal top displacement and SF_{urm} is the shear force at the base of the URM wall. F_e is the total force applied by the two horizontal actuators and SF_{rc} is the shear force at the base of the RC wall. *N1* and *N2* are the vertical forces measured at the base of the URM wall (Figure 9b) and *W* is the total axial load applied at the top of the URM and RC wall by the four hollow core jacks.

M3 is the moment that the rotational hinges (GX45F), part of the system to measure the horizontal reaction force, transmit. The equation, provided by the hinge producer (SKF, http://www.skf.com), assumes friction equal to 0.05 [-] and d_m (diameter of the hinge) equal to 89.2 mm. *N3* is the parasitic force generated by the two rotational hinges and l_h is the distance between the two hinges that is equal to 174 mm (Figure 9a).

ΔN is the variation in axial force at the base of the walls due to the applied horizontal force ($\Delta N_{rc} = -\Delta N_{urm}$). N_{urm} and N_{rc} are the axial forces at the base of the two walls and are calculated by adding to the variation of the axial force ΔN the vertical forces applied by the hollow core jacks plus the self-weight of the test unit and parts of the test set-up supported by the walls.

M_{urm} is the moment at the base of the URM wall. *a*, *b* and *c* are the lever arms of the reaction forces with respect to the centre of the URM wall (point A, Figure 9b) and are equal to 1200 mm, 2445 mm and 220 mm, respectively. *OTM* is the total overturning moment and d_1 and d_2 correspond to the height of the two actuators and are equal to 3520 mm and 1710 mm. *Tl* is the contribution of the RC beams to *OTM* and l_{aw} is the distance between the two wall axes, which is equal to 2400 mm. M_{rc} is the moment at the base of the RC wall.

Drift is the average drift of the specimen (H_{top} is equal to 3520 mm). Channels 115 to 118, 124 and 127 to 131 were shifted to zero in such a way that the measurements at the beginning of LS1 correspond to zero (*index* = 601 for TU1; *index* = 2501 for TU2).

The processed conventional data are saved in a txt file. The first two lines of the file assign the name of the channel and the unit. When channels are empty, the numerical values are replaced with "NaN".

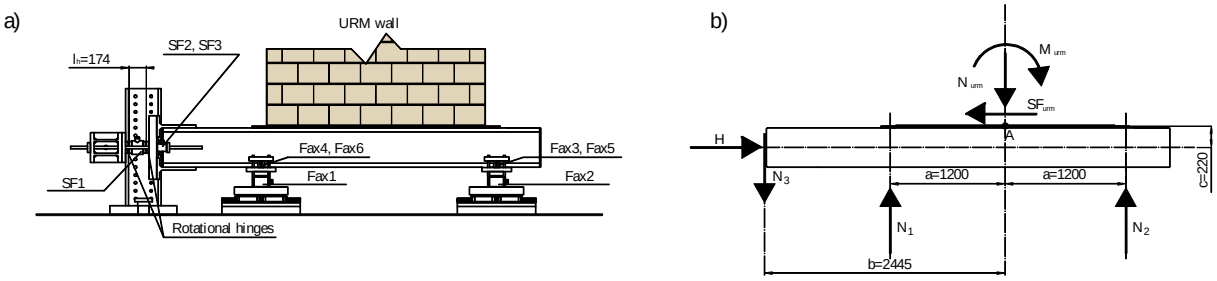

Figure 9: Steel beam with the system to measure the horizontal and vertical forces at the base of the

URM wall (a); free body diagram of the steel beam with reaction forces (b). All dimensions in mm.

3.2.6 Processed optical measurement data

The data acquired from the two position sensors were merged together and the coordinate system was rotated and shifted to align the axes with the x- and y-axes as indicated in Figure 6. The LEDs glued onto the URM walls were then re-numbered from 1 to 448 from the bottom-north corner of the first storey (Marker_1) to the top-south corner of the second storey (Marker_448). These markers are then followed in the numeration by the markers glued onto the steel foundation, the RC beams and the C-section beams. The optical measurement data at each load step were averaged and condensed to one measurement point. The processed optical data are saved in a txt file. The first two lines of the file assign the name and the coordinate measurement of each LED and the following lines store the -x, -y and -z coordinates at each load step starting from LS0.

4 Additional photos describing the progressive damage in the test units

This section provides photos describing the damage evolution of the two specimens for several limit states associated with the nominal drifts summarised in Table 2.

Table 2: Limit states and corresponding nominal drifts

Limit state	TU1	TU2
No significant stiffness degradation of the URM walls	+0.1%	+0.1%
Horizontal load failure of the test units for the negative loading direction	-0.3%	-0.4%
URM wall heavily damaged (*) for the positive loading direction	+0.6%	+0.6%
Onset of horizontal load failure of the units for the positive loading direction	+0.95%	+1.12%

(*): strength of TU1's URM wall dropped by ~20%; crack pattern of TU2's URM wall mainly developed

4.1 TU1

4.1.1 No significant stiffness degradation of the URM wall (δ = +0.1%)

At an average drift δ equal to +0.1%, very small shear cracks following the joints started forming in the URM wall (Figure 10a). In the RC wall, small flexure cracks in the first storey were detected (Figure 10b).

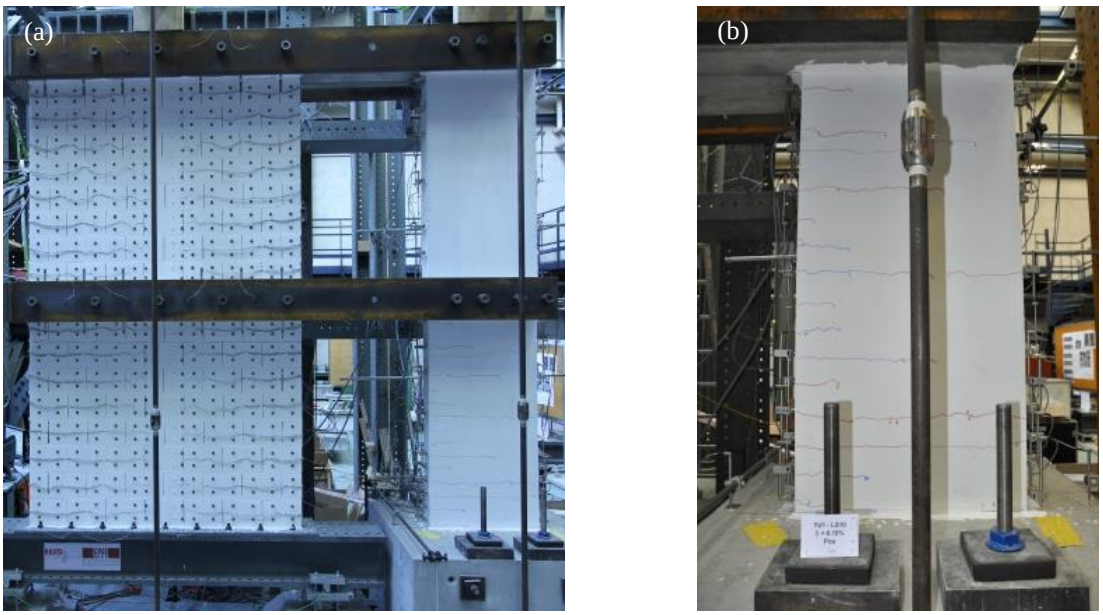

Figure 10: Crack pattern at LS10, δ = +0.1%. (a) specimen; (b) RC wall, first storey.

4.1.2 Horizontal load failure of the unit for the negative loading direction (δ = -0.3%)

At LS27, when the target average drift of δ = -0.3% was reached, the horizontal load was stopped, photos were taken and cracks were marked. In the first storey of the URM wall, inclined shear cracks and the onset of toe-crushing were observed. In the second storey of the URM wall, only thin inclined shear cracks appeared (Figures 11a, 12a and 12b). During the crack marking, a relaxation in the URM wall occurred: the number of cracks in the compressed corner grew, the shear strength of the URM wall rapidly decreased and the specimen attained horizontal load failure. In order to avoid axial load failure of the URM wall, the horizontal load was reduced to zero. Figures 11b, 12c and 12d show the specimen crack pattern after the strength degradation of the URM wall.

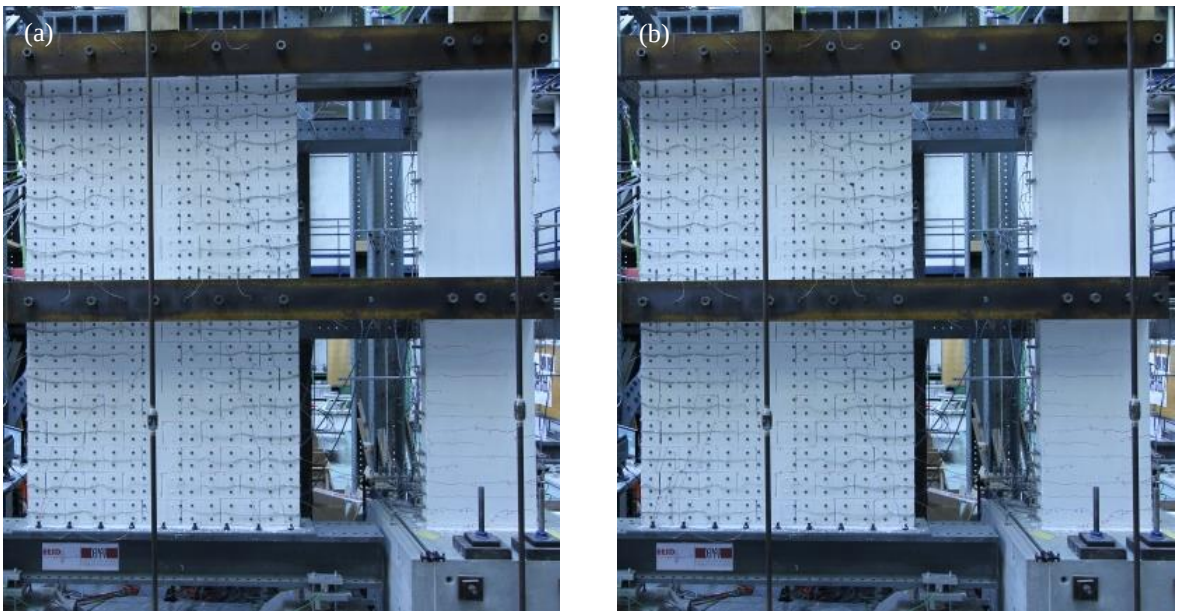

Figure 11: Specimen crack pattern at LS27, δ = -0.3%. Before (a) and after (b) the horizontal load failure.

Figure 12: Crack pattern at LS27 (δ = -0.3%) of the compressed corner of the first storey of the URM wall. Before (a, b) and after (c, d) the horizontal load failure.

4.1.3 URM wall heavily damaged for the positive loading direction (δ = +0.6%)

At LS31, the URM wall was heavily damaged: steeply inclined shear cracks passing mainly through bricks were detected in both storeys of the URM wall (Figures 13a, 13c and 13d). At this load step, the strength of the URM wall dropped by around 20%. Figure 13b shows that the extent of the curvature penetration of the first storey RC beam into the URM wall was around 60 cm.

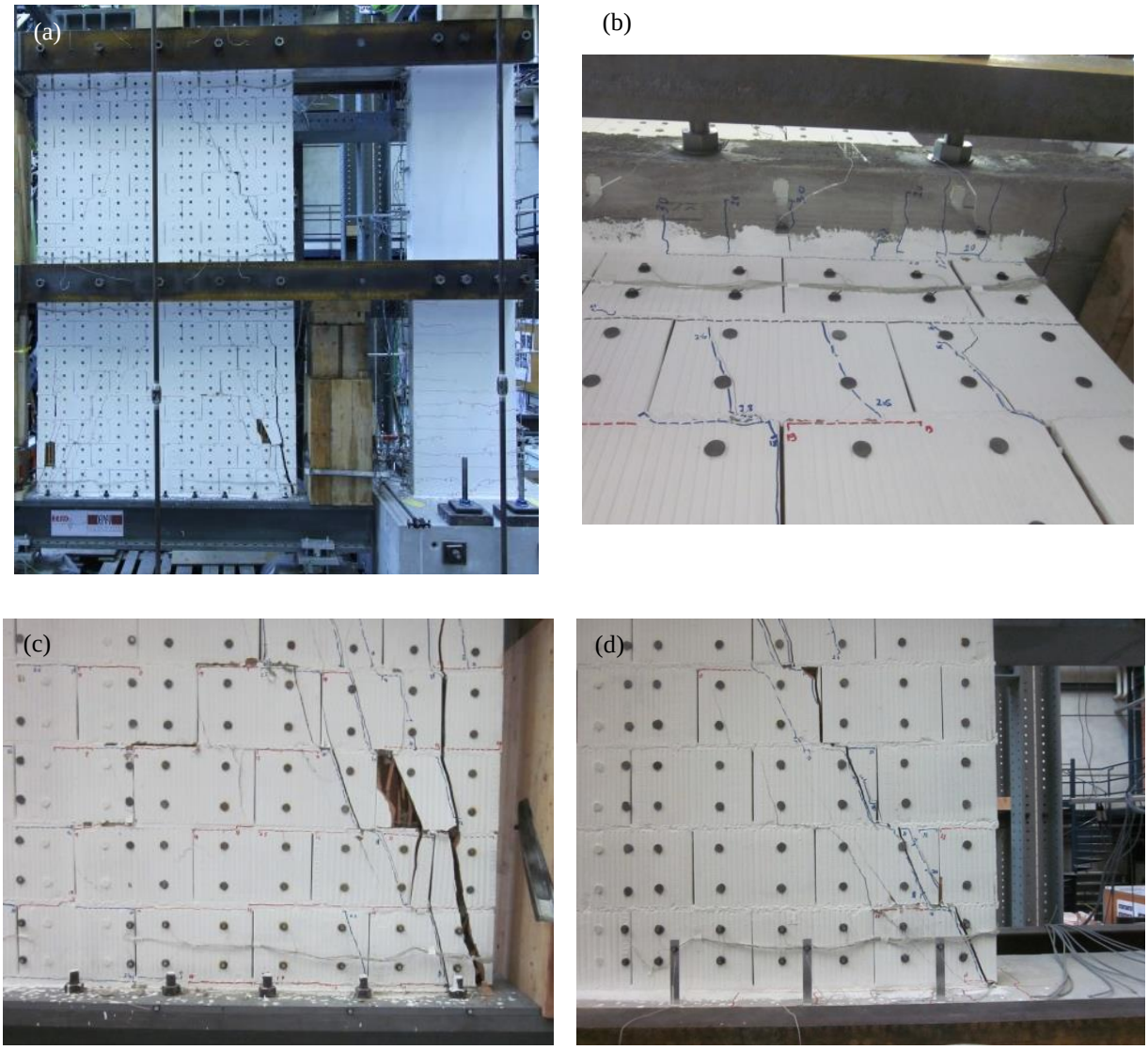

Figure 13: Crack pattern at LS31, δ = +0.6%. (a) specimen; (b) RC first storey beam, curvature penetration into the URM wall; (c, d): compressed corner of the first and second storey of the URM wall.

4.1.4 Horizontal load failure of the unit for the positive loading direction (δ = +0.95%)

Horizontal load failure of TU1 occurred during the half cycle with δ = +0.95% (LS33), i.e., at a drift demand around three times the drift capacity for loading in the negative direction (δ = -0.3%).

The axial load failure of the first storey of the URM wall, due to the crushing of the compressed toe, was quickly followed by the horizontal load failure. Figure 14a shows that in the URM wall the cracks were not concentrated in the bottom storey, as is typical for URM walls, but they also spread up to the second storey because of the presence of the RC wall that changed the global deformed shape of the system. At the same load step (LS33), the RC wall was still in the pre-peak response and only some of the longitudinal reinforcing bars at the north edge had yielded. The crack pattern of the first storey of the RC wall consisted of horizontal flexure cracks plus some shear-flexure cracks that started developing in the previous cycle (LS32, δ = +0.8%), as seen in Figure 14b. The second storey of the RC wall exhibited only small cracks in the construction joints. Figures 14c and 14d show the detail of the crack pattern after the failure of the first and second storey of the URM wall.

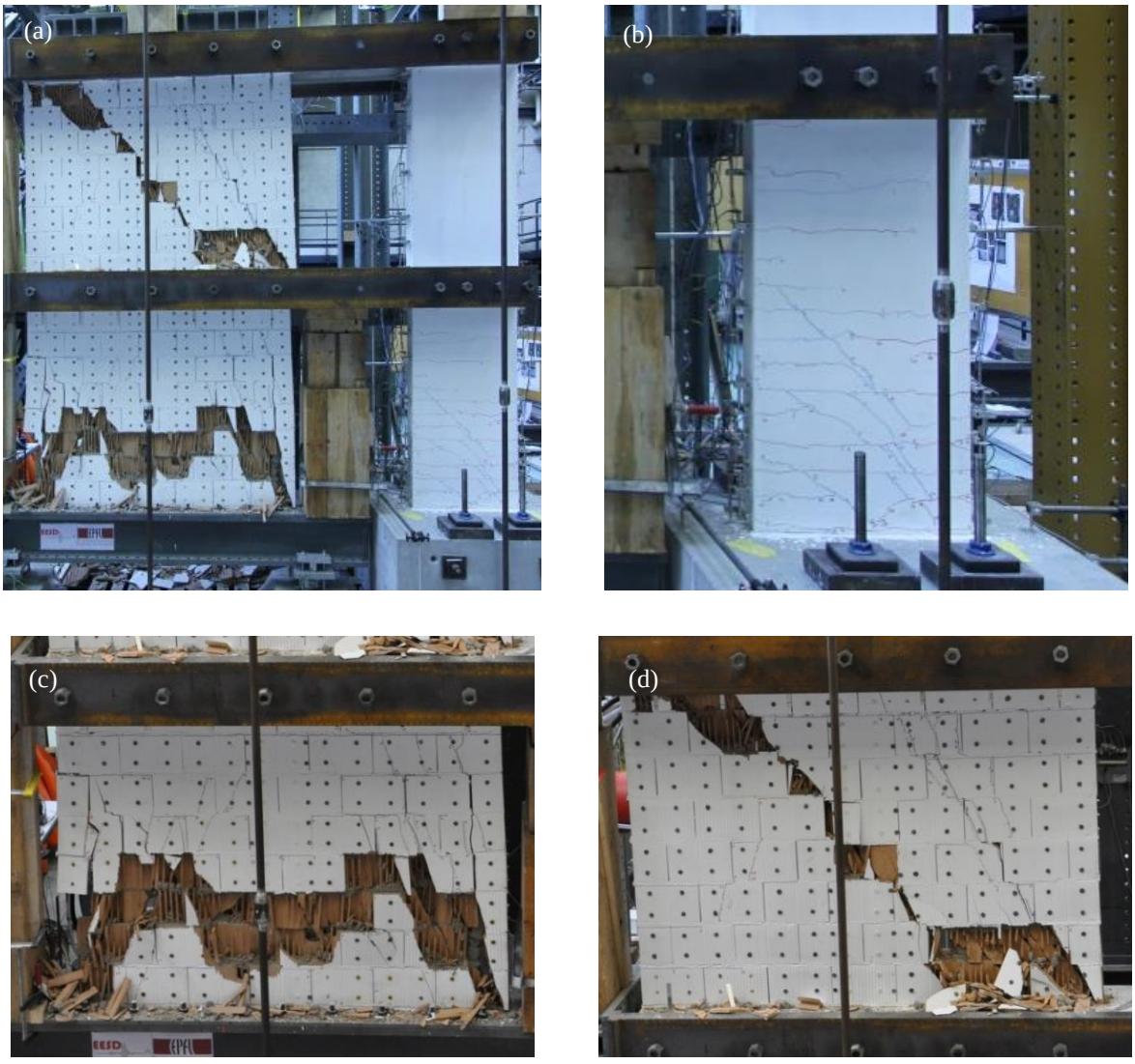

Figure 14: Crack pattern at LS33, δ = +0.95%. (a) specimen; (b) RC wall, first storey; (c, d) close-ups of the first and second storey of the URM wall.

4.2 TU2

4.2.1 No significant stiffness degradation of the URM wall (δ = +0.1%)

At an average drift δ equal to +0.1%, the URM wall displayed only small horizontal cracks (Figure 15a). In the first storey of the RC wall, only small flexure cracks were observed (Figure 15b).

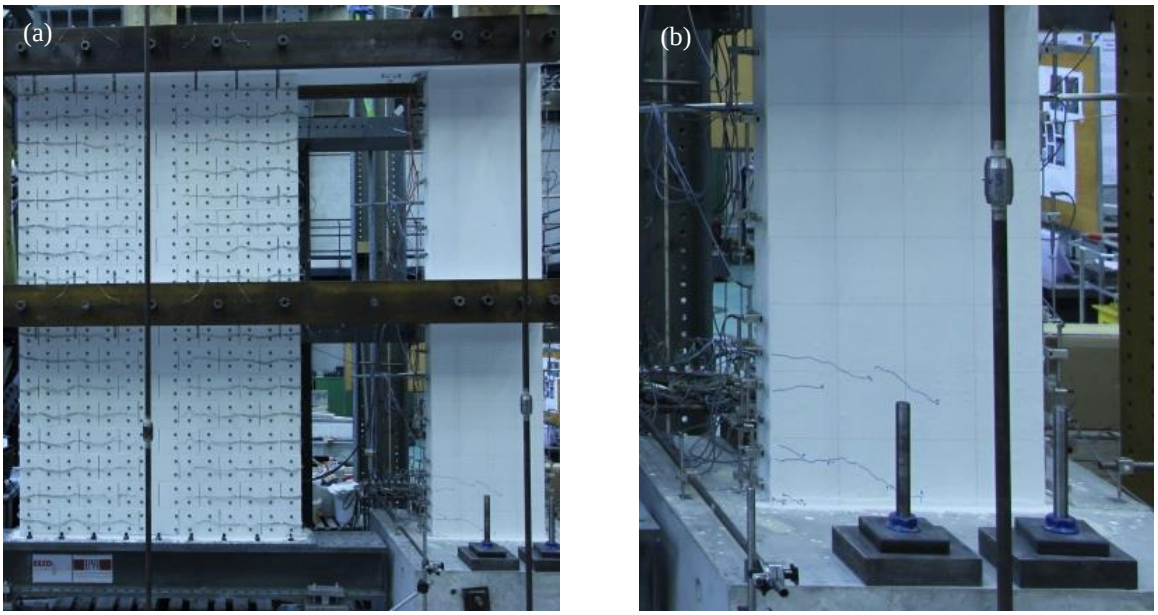

Figure 15: Crack pattern at LS10, δ = +0.1%. (a) specimen; (b) RC wall, first storey.

4.2.2 Horizontal load failure of the unit for the negative loading direction (δ = -0.4%)

At LS33, when the target average drift of δ = -0.4% was reached, the shear strength of the URM wall dropped by 10% and the horizontal force was immediately reduced to zero to avoid the axial load failure of the URM wall. The crack pattern in the URM wall comprised diagonal cracks in the first storey pointing towards the compressed corner (Figures 16a and 16c): the onset of the toe-crushing was also observed (Figure 16d). The second storey of the URM wall was crossed by just one thin shear crack in addition to a horizontal crack at the base of the second storey. In the first storey of the RC wall, shear-flexure cracks were observed (Figure 16b).

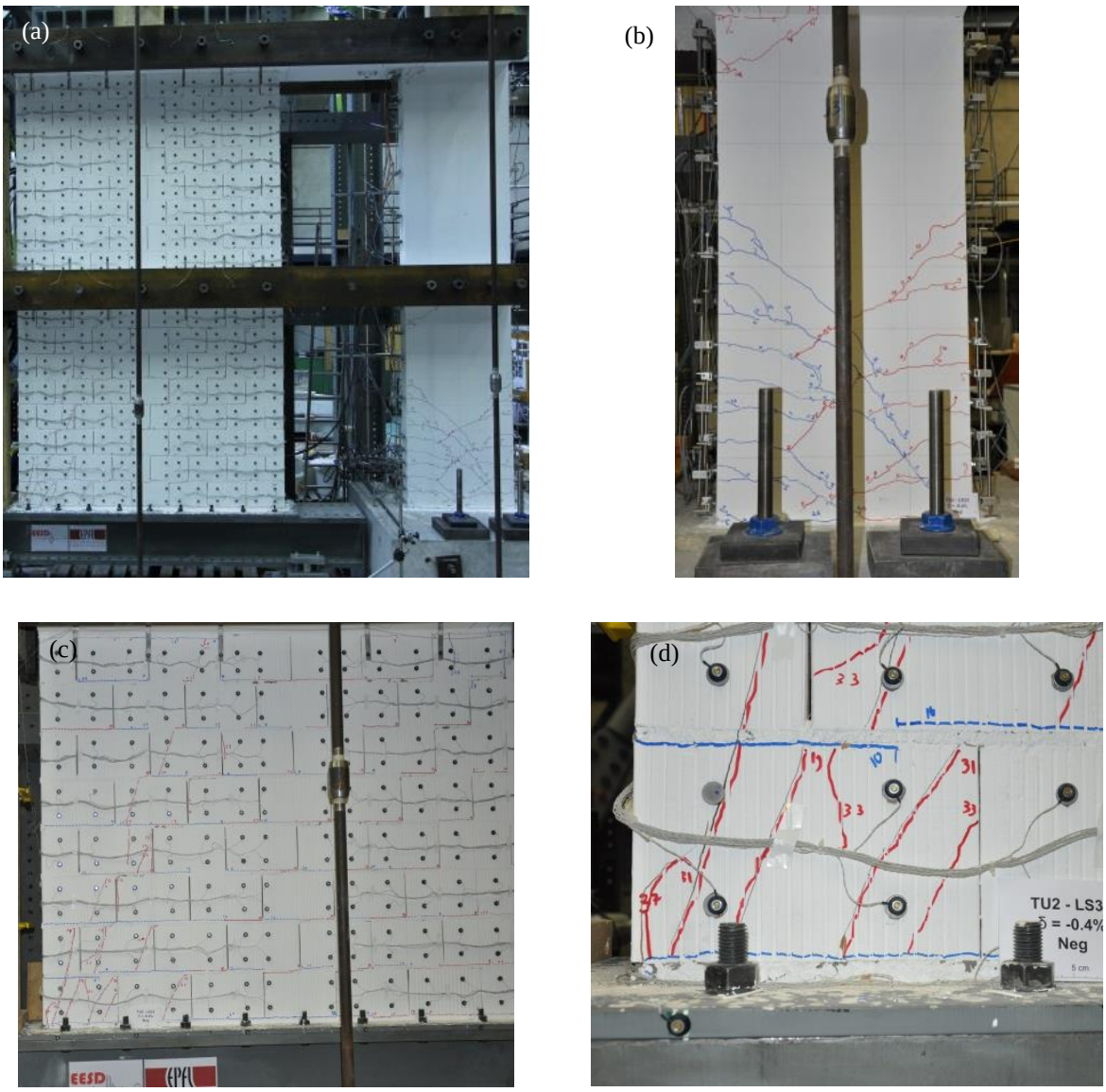

Figure 16: Crack pattern at LS33, δ = -0.4%. (a) specimen; (b, c) crack pattern at the bottom storey of the RC and URM wall; (d) compressed corner of the first storey of the URM wall.

4.2.3 URM wall heavily damaged for the positive loading direction (δ = +0.6%)

At LS35, the crack pattern was mainly developed in the URM wall (Figure 17a). In the bottom storey of the URM wall, steeply inclined shear cracks were detected. In addition, vertical splitting cracks due to the rocking motion appeared at the toe of the wall (Figure 17c). In the second storey of the URM wall, a stair-stepped crack passing though the mortar joints formed and splitting cracks in the compressed corner were observed (Figure 17d). Figure 17b shows that the extent of the cracked part of the RC beam penetrating into the URM wall was around 60 cm.

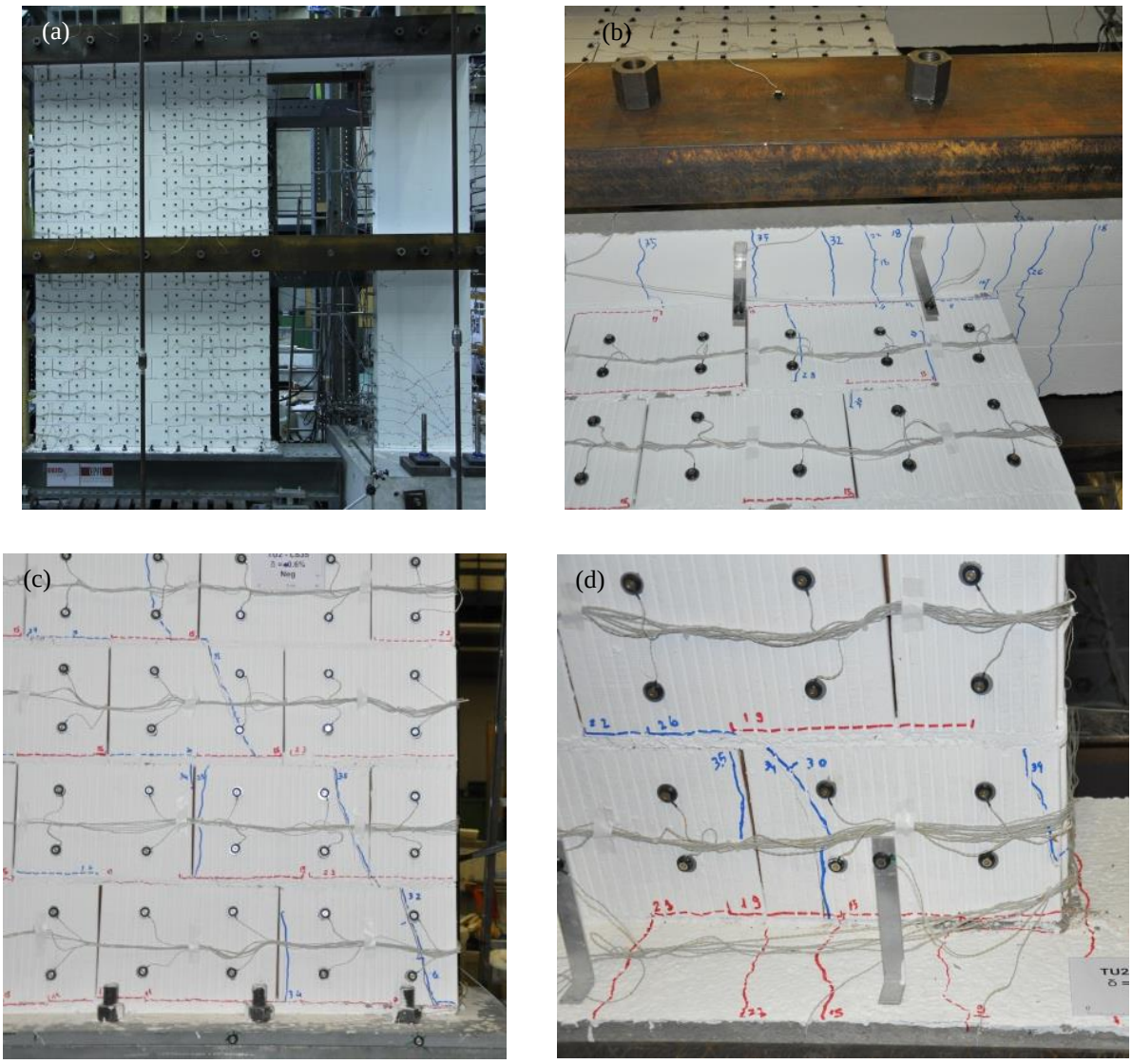

Figure 17: Crack pattern at LS35, δ = +0.6%. (a): specimen; (b) RC first storey beam, curvature penetration into the URM wall; (c, d): compressed corner of the first and second storey of the URM wall.

4.2.4 Onset of horizontal load failure of the unit for the positive loading direction (δ = +1.12%)

Horizontal load failure of TU2 occurred during the half cycle with δ = +1.12% (LS38), i.e., at a drift demand around three times the drift capacity for loading in the negative direction (δ = -0.4%). Figure 18a shows that, similarly to TU1, in the URM wall the cracks were not concentrated in the bottom storey, but they also spread up to the second storey because of the presence of the RC wall that changed the global deformed shape of the system. Figure 18b shows that the RC wall was far from failure and only shear-flexure cracks in the first storey were observed. As for TU1, the second storey of the RC wall exhibited only small cracks in the construction joints.

Steeply inclined shear cracks passing mainly through bricks were detected in the bottom storey of the URM wall (Figure 18c). Toe-crushing of the compressed corner was also observed. In the second storey of the URM wall, the plastic deformations were mainly concentrated in one single stair-stepped crack that crossed the wall (Figure 18d). Toe-crushing of the compressed corner was also observed in the second storey.

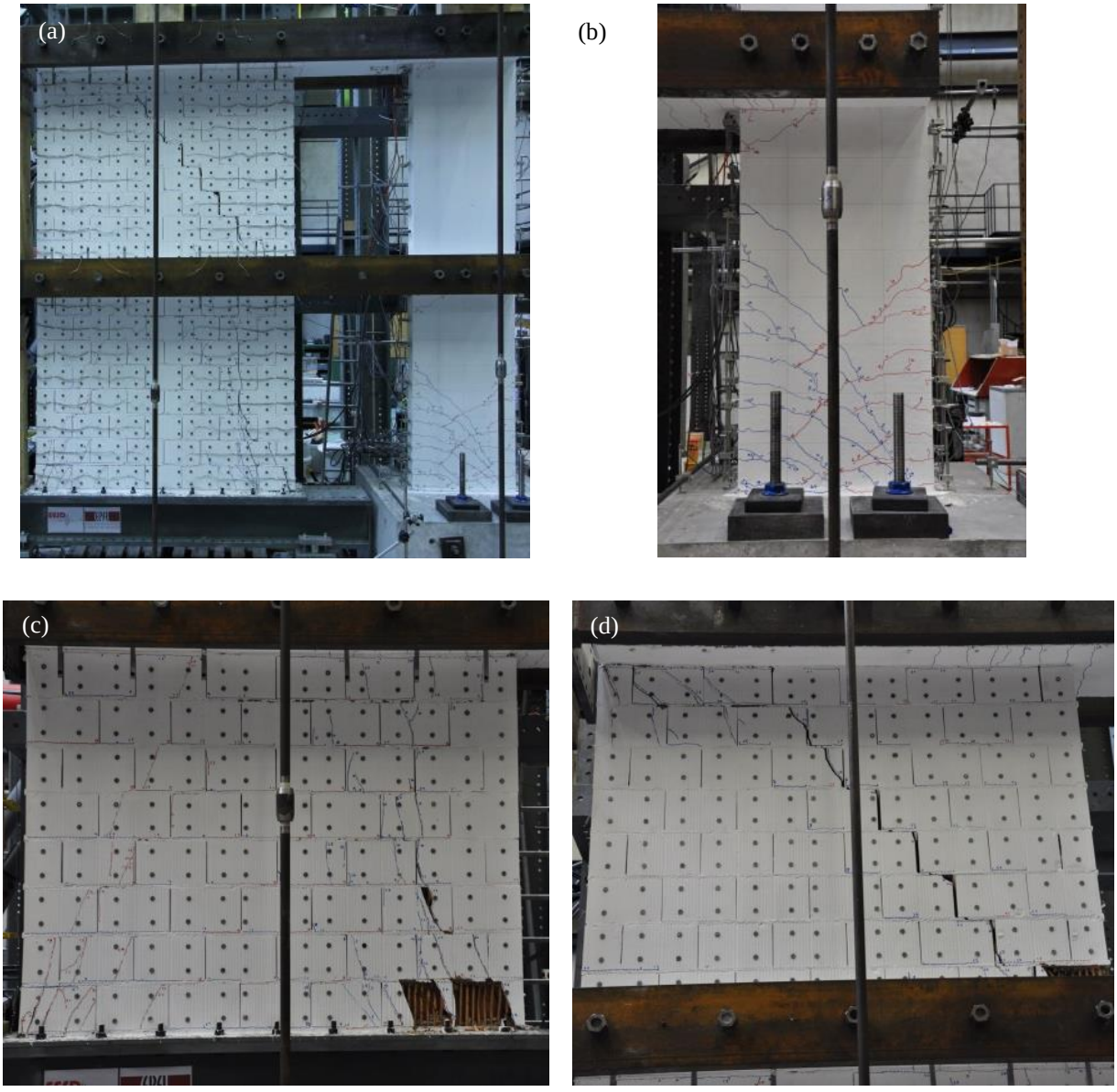

Figure 18: Crack pattern at LS38, δ = +1.12%. (a) specimen; (b) RC wall, first storey; (c, d) close-ups of the first and second storey of the URM wall.

5 References

NDI. [2009] “Optotrak Certus HD”, *Northern Digital Inc.*, Waterloo, Ontario, Canada, http://www.ndigital.com/industrial/certushd.php.